12-15-1991

Evidence for Proximal Control of Ligand Specificity in Hemeproteins: Absorption and Raman Studies of Cryogenically Trapped Photoproducts of Ligand Bound Myoglobins

Mark R. Chance
Case Western Reserve University, mark.chance@case.edu

Author(s) ORCID Identifier:

iD Mark R. Chance

Recommended Citation

Evidence for proximal control of ligand specificity in hemeproteins: absorption and Raman studies of cryogenically trapped photoproducts of ligand bound myoglobins ☆

A.M. Ahmed [a], B.F. Campbell [a], D. Caruso [a], M.R. Chance [b], M.D. Chavez [c], S.H. Courtney [a], J.M. Friedman [a,1], I.E.T. Iben [a], M.R. Ondrias [c] and M. Yang [a]

[a] *Department of Chemistry, New York University, New York, NY 10003, USA*
[b] *Department of Chemistry, Georgetown University, Washington, DC 20057, USA*
[c] *University of New Mexico, Albuquerque, NM 87131, USA*

The absorption and resonance Raman spectra of cryogenically trapped photoproducts of oxy and carboxy derivatives of myoglobin (Mb) are compared and analyzed in an attempt to understand the structural basis for ligand specificity in hemeproteins. Pulsed and cw excitations over a wide temperature range are used in order to differentiate between kinetic hole burning (KHB), optical pumping of structural relaxation, and spontaneous relaxation effects. Using these techniques, we are able to correlate changes in the absorption spectrum (band III at ≈ 760 nm) with low-frequency Raman bands. Based on these correlations we are able to determine which proximal heme pocket parameters are participating in KHB and optical pumping phenomena. Differences in the spectra of the ligand specific photoproducts have revealed differences in the populations of conformational substates (CS) that participate in the geminate recombination (process I) at cryogenic temperatures. A model is presented that relates the ligand specific spectral differences to structural and functional differences in the bound protein. What emerges is evidence that Mb and hemoglobin (Hb) can differentiate between O_2 and CO based on proximal control of the bond forming step between the ligand and the iron.

1. Introduction

Oxygen and carbon monoxide are comparably sized molecules and yet their binding properties to hemoglobin and myoglobin differ in several significant ways [1]. Despite numerous studies there are still many unanswered questions regarding both the extent to which these two ligands differ and the physical basis for differences. It is known that the on and off rates for these two ligands differ. The measured on and off rates can have contributions from any of the several steps that are thought to comprise the overall binding and dissociation process [2–4]. In addition to those steps directly coupled to bond formation and dissolution, there are also steps such as

ligand motion from the solvent into the protein and ligand escape from the distal heme pocket. The latter are expected to be less closely connected to the dynamics associated with the iron ligand bond. In this work we focus on those processes that are anticipated to be closely coupled to iron–ligand bond formation and dissolution.

Ligand heme interactions have been effectively studied by photodissociating ligand bound hemeproteins and monitoring the recombination process. The pioneering work of Frauenfelder and co-workers demonstrated that under cryogenic conditions the photodissociated ligand can remain trapped within the heme pocket [2]. Subsequent recombination occurs entirely from within the protein. Recombination from within the protein is termed geminate recombination. Geminate recombination allows one to focus on dynamics leading up to and including bond reformation starting with the ligand in the heme pocket. The same type of isolated recombination can

be studied at ambient temperatures but with the added complication that at some point after photodissociation there is the competing process of ligand escape from the heme pocket. There is the added issue that the rate and extent of any structural relaxation occurring subsequent to ligand dissociation may be strongly temperature dependent; consequently, the structure that modulates rebinding at cryogenic temperatures may be different from that at higher temperatures where the relaxation can occur on a time scale comparable to or faster than ligand rebinding.

The early photodissociation experiments reveal that for both hemoglobin and myoglobin at ambient temperatures the quantum yield for photolysis is considerably higher for carbon monoxide relative to oxygen [1]. Subsequently it was shown that geminate recombination (GR) on the nanosecond [5–8] and faster [9–13] time scales accounts for ligand and protein specific differences in the "steady state" quantum yield. In these ambient temperature studies it is observed that the O_2 ligand undergoes far more GR than does CO. The overall picture that emerges from the room temperature studies is that oxygen geminately recombines both more rapidly and more extensively than CO over a time course covering up to six decades in time following the dissociative step.

At cryogenic temperatures the geminate rebinding in Mb displays features that are seemingly at odds with the solution phase results. A comparison of the GR starting at several microseconds after photolysis reveals similar rebinding parameters for O_2 and CO[14]. This finding led to the suggestion that the geminate rebinding process for these two ligands is controlled by comparable energy barriers and entropic factors [14]. It is clear that this similarity between O_2 and CO holds for that fraction of the photoproduct population that rebinds on a microsecond or slower time scale. For O_2 this represents less than half of the total photodissociated population for the temperatures used in these studies [15]. For the CO derivative nearly a hundred percent of the population of photoexcited material is contributing to the observed rebinding process.

Resonance Raman [16] and transient absorption [15] studies show that in addition to a CO like slow rebinding population of O_2 there is a fraction of the population that can not be photodissociated with 10 ns and 30 ps pulses, respectively, under cryogenic

conditions where MbCO or HbCO is completely dissociated. As much as sixty percent of the oxy sample cannot be photolyzed with a 30 ps laser pulse even with repetitive and extended excitation. Thus at cryogenic temperatures there are two noninterconvertable photoproduct populations for the oxy derivatives: one with very fast geminate or electronic relaxations and the other that rebinds O_2 with rates comparable to CO.

The general thrust of the present work is directed at two fundamental questions. The first question is to what extent are the two populations of HbO_2 and MbO_2 structurally distinct in the sense that one can identify some structural feature that determines if a given molecular conformation will be either CO like or "nonphotolyzable". The second question is how similar are the structures of the photoproducts of the carboxy and oxy derivatives of Mb and Hb. In particular, does the slow rebinding photoproduct population derived from the oxy derivative have the same distribution of conformations as that derived from corresponding carboxy derivatives. Contained within these questions are such issues as the mechanism by which the protein structure discriminates between ligands and the relationship between protein structure and ligand reactivity.

These questions and issues raise the pragmatic problem of which element of the protein structure does one focus upon. It has long been thought that discrimination between ligands by the protein occurs via interactions between the ligand and the distal heme pocket (distal effects). More recently it has also been argued that O_2 and CO have different rates of entry and escape from the distal heme pocket [17]. None the less there are indications that the bond forming step is not influenced by distal effects [18]. Instead modulation of the iron by the protein (proximal effects) appears to exert control at that level of reactivity [18]. Under cryogenic conditions employed in this study the iron ligand bond forming step is isolated; consequently we have chosen to spectroscopically probe the proximal heme environment within the different photoproduct populations. Two spectral bands are used in this study as probes of the proximal heme environment in cryogenically trapped photoproducts. In the absorption spectra of the five coordinate ferrous photoproducts, we focus on a protein structure sensitive porphyrin to iron charge

transfer band [19,20]. This band is centered at approximately 760 nm and is labeled band III. The line shape has an inhomogeneous contribution attributed to a distribution of iron displacements within the photoproduct population [17,21–23].

Resonance Raman is used to provide greater detail with respect to degrees of freedom associated with the iron which are sensitive to structural changes in the protein [24]. More importantly the Raman data is useful in establishing which degrees of freedom modulate the iron displacement reflected in band III. Together [23], the 760 nm absorption band and the iron histidine stretching mode [23–30] in the Raman spectrum provide a detailed picture of the proximal heme pocket parameters that includes both the range of iron positions and the conformation specific determinants of this coordinate.

Kinetic hole burning experiments utilizing the 760 nm band and the Fe–His stretching mode are used in this study to connect structure to rebinding properties. The KHB technique [21–23,31] is derived from several concepts. The use of the term conformation in the above paragraphs is not entirely appropriate under all experimental conditions. Frauenfelder and co-workers [2] have used the concept of conformational substates (CS) to explain the power law rebinding kinetics observed for hemeproteins at cryogenic temperatures. Instead of a single unique conformation for a given protein in solution, there is a distribution of CS whose members have roughly the same overall conformation but differ in the specific details of the atomic coordinates. Associated with the distribution of CS is a distribution of reactivities: each CS having a well defined structure and reactivity. At ambient temperatures the CS are thermally interconverting sufficiently fast that for microsecond or longer processes an average conformation is the appropriate description for the relevant structure. At cryogenic temperatures, however, the thermal interconversion eventually ceases resulting in a frozen distribution. If there is a spectral band having a spectral property such as wavelength that varies systematically with the conformation, then the spectral band may show inhomogeneous broadening as in the case of band III [17,21–23]. Each member of the distribution of CS has a distinct iron displacement with an associated peak wavelength for its corresponding band III. If different CS contributing to the inhomogeneous

broadening in a spectral band of the photoproduct also have different recombination rates then as the recombination proceeds that spectral band will initially lose intensity from that segment of the line shape derived from the fastest recombining CS. KHB has been observed in band III of photoproducts derived from MbCO [17,21,22] and HbCO [23] at cryogenic temperatures.

The present study uses KHB in several ways. The slower (CO like) population of oxy derived photoproducts is compared to CO derived populations with respect to KHB in band III in order to test whether the same distributed structural parameter contributes to the control of recombination for both ligands. In an attempt to determine if there is a structural basis for the low photodissociation QY of O_2 bound Mb and Hb, we also compare band III from fully photolyzed CO samples to maximally photolyzed O_2 samples at liquid helium temperatures where only 40% of the O_2 sample can be photodissociated [15]. The resonance Raman spectra of these different populations are also generated in anticipation of being able to determine the structural coordinate responsible for the iron displacement which is probed in the band III studies. Ancillary issues are also addressed. The structure of the ligand bound protein differs from that of the equilibrium deoxy protein. Thus at cryogenic temperatures or at early times following photodissociation, the photoproduct will consist of a five coordinate heme surrounded by an unrelaxed or partially relaxed globin. Since the relaxed and unrelaxed photoproduct structures are expected to have different recombination properties and since the recombination rates and relaxation rates are likely to be temperature dependent, it is important for our purposes to characterize the dynamic and static processes that determine the temperature dependent spectra from the photoproduct.

The results of this study show that:

(1) The spectra from maximally photodissociated populations of oxyhemeproteins resemble the spectra from the corresponding CO derived sample that has already undergone partial recombination (i.e. the oxy photoproduct spectra look like a kinetically hole burned CO sample).

(2) The population of the slow "CO" like oxy photoproduct is comprised of CS that are more deoxy like than those derived from the corresponding CO sam-

ple indicating that the recombination rate for a given photoproduct CS is ligand dependent.

(3) The extent to which structural relaxation, optical pumping and kinetic hole burning contribute to the temperature dependent changes in the photoproduct Raman spectra is exposed using a combination of cw and nanosecond excitations.

(4) The Raman data indicate that both the tilt angle and the azimuthal angle of the proximal histidine play a role in establishing the distribution of iron displacements responsible for the KHB in band III. These results are used to develop a model in which protein induced O_2–CO differences in geminate recombination originate from proximal control.

2. Methods and materials

The methods for obtaining the band III optical spectra and performing the KHB protocols are described in our earlier work [21,23]. The protocols for preparing samples and taking the Raman spectra are also described in earlier work [24]. The samples used in the band III studies are in standard 75% gycerol-water glasses whereas the Raman data was obtained primarily from frozen aqueous solutions due to interference of fluorescence from the glycerol samples. Potassium phosphate and Tris buffers were used to create the high- and low-pH solutions, respectively.

3. Results

3.1. Band III

Fig. 1 shows the kinetic hole burning (KHB) pattern for oxy and carboxy Mb and HbA (at pH 6 + IHP). It can be seen that in all instances the normalized spectrum of the $\approx 80\%$ recombined sample appears blue shifted with respect to the maximally photodissociated sample. Figs. 2 and 3 show respectively for Mb and Hb (at low pH) a comparison of band III for the maximally photodissociated oxy and carboxy forms of these proteins. In both instances the normalized band III from the oxy sample which is only $\approx 40\%$ photodissociated when maximally illu-

minated [15] is blue shifted from the fully photo-lyzed CO sample.

3.2. Raman

The low-frequency cw Raman spectrum of the photoproduct of oxyMb,$Mb^*(O_2)$ differs from that of the photoproduct of COMb,$Mb^*(CO)$. The major noticeable difference is in ν(Fe–His) at ≈ 230 cm^{-1}. For the former, the intensity of ν(Fe–His) is higher relative to the pure heme bands and the frequency slightly lower. This pattern persists at all temperatures between 2 and 150 K. As a result, $Mb^*(O_2)$ has a more deoxy like spectrum compared to $Mb^*(CO)$ at any given temperature in that range. A comparison of the spectra at 80 K from $Mb^*(O_2)$, $Mb^*(CO)$, and deoxy Mb(Mb) is shown in fig. 4. Also shown is a spectrum of $Mb^*(CO)$ using a pulsed (10 ns) excitation at the same wavelength as the cw laser. In terms of relative intensities and frequency, it can be seen that the cw spectrum from $Mb^*(O_2)$ and the pulsed $Mb^*(CO)$ spectrum are closer to that of Mb than is the cw spectrum of $Mb^*(CO)$. In going from 2 to 220 K, the cw Raman spectra from both photoproducts show similar changes.

In going from 2 to 80 K the intensity in the Raman spectrum of the iron-proximal histidine stretching mode, ν(Fe–His), increases relative to the heme modes for the sperm whale $Mb^*(CO)$ [24,29,30]. This pattern extends to other Mbs such as elephant and tuna Mbs [31]. With still further increases in temperature the relative intensity increase of ν(Fe–His) increases still further and a shift towards lower frequency becomes apparent. Careful visual inspection of the spectra suggests that as the relative intensity of ν(Fe–His) increases in going from 2 to 220 K the peak frequency only starts to be noticeably shifted above 80 K. Two series of spectra, obtained using a cw and a pulsed excitation (10 ns, 50 Hz) at the same wavelength and having the same average power (≈ 20 mW) are shown in figs. 5 and 6, respectively. Clear differences are seen between the cw and pulsed spectra at a given temperature. Fig. 7 shows a plot of the relative intensity of ν(Fe–His) as a function of temperature for the two excitations as well as the cw spectra from Mb and $Mb^*(O_2)$. Fig. 8 shows a similar plot but for the frequency. The pulsed data in the plots are derived from spectra taken with lower pulse
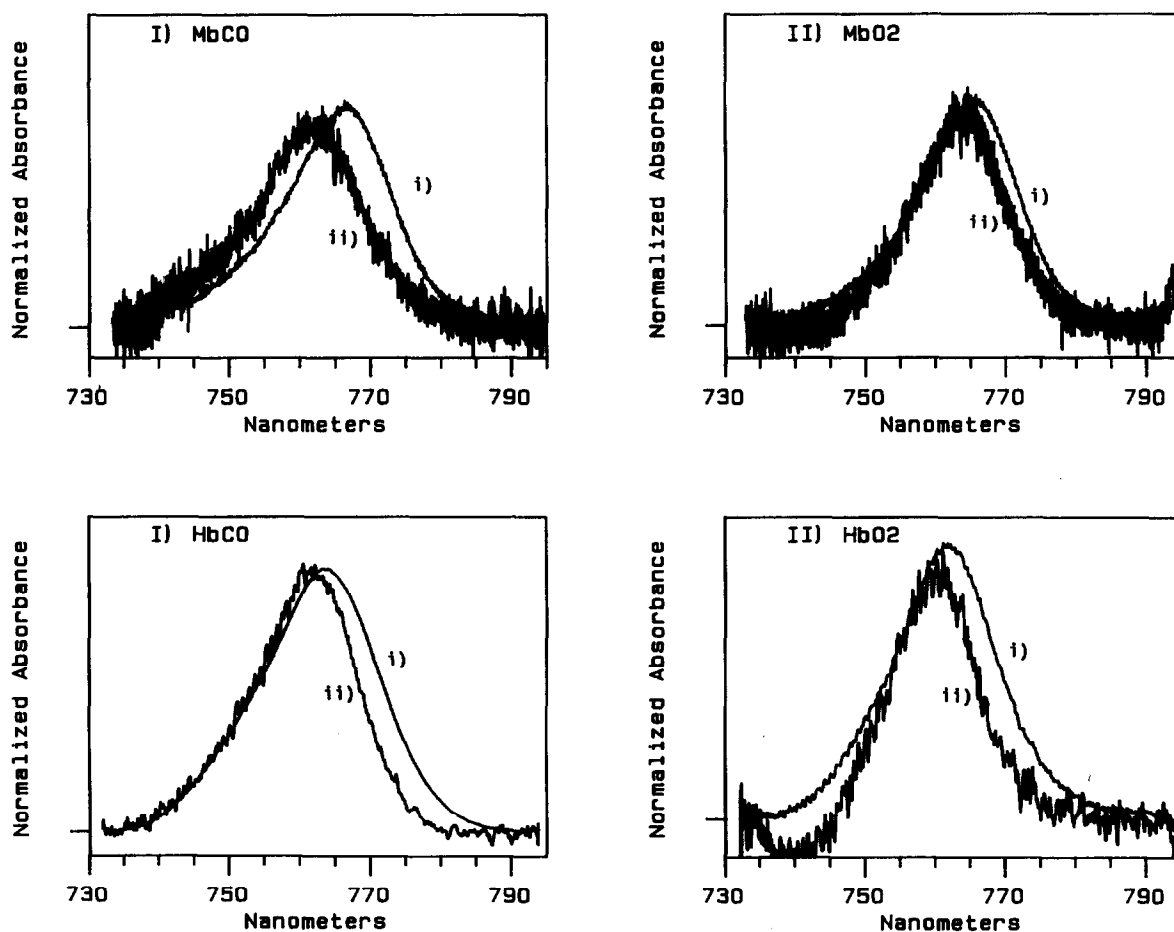
Fig. 1. A comparison of band III for maximally photodissociated and partially recombined samples of CO and O_2 derivatives of Mb and HbA (at pH 6+IHP). The intensities of band III for the recombined samples (80% recombined with respect to the starting maximally photodissociated samples) are normalized to those of the maximally photodissociated samples. In each case i) refers to the maximally photodissociated sample, and ii) refers to the sample that has undergone partial recombination.

energies than used to generate the spectrum shown in fig. 4. Increasing the pulse energy increases the relative intensity of ν(Fe–His) at the lower temperatures as can be seen in comparing figs. 7 and 9. It can also be seen that the large changes which begin for the cw Mb*(CO) spectrum at ≈ 100 K are not apparent in the pulsed spectra and that the changes seen for the CO sample are apparent in the O_2 sample at lower temperatures. Thus at intermediate temperatures the Mb*(O_2) spectrum resembles a higher temperature Mb*(CO) spectrum and the "pulsed" spectrum resembles the cw spectrum taken from the same sample but at a lower temperature. The break in the oxy data

stems from the poor quality of the photoproduct data for this sample at the higher temperatures due to the drastically reduced population of photoproduct from either a reduced QY or enhanced process I. In other samples it is clear that at 120 K the Mb*(O_2) spectrum is substantially closer to the Mb spectrum than even the 160 K Mb*(CO) spectrum.

Convoluted into the temperature dependence of the photoproduct spectra is a pure thermal effect which appears to cause a decrease in most low-frequency Raman bands with increasing temperature. To separate out this effect on ν(Fe–His), we plot in fig. 10 the temperature dependence of a relaxation function
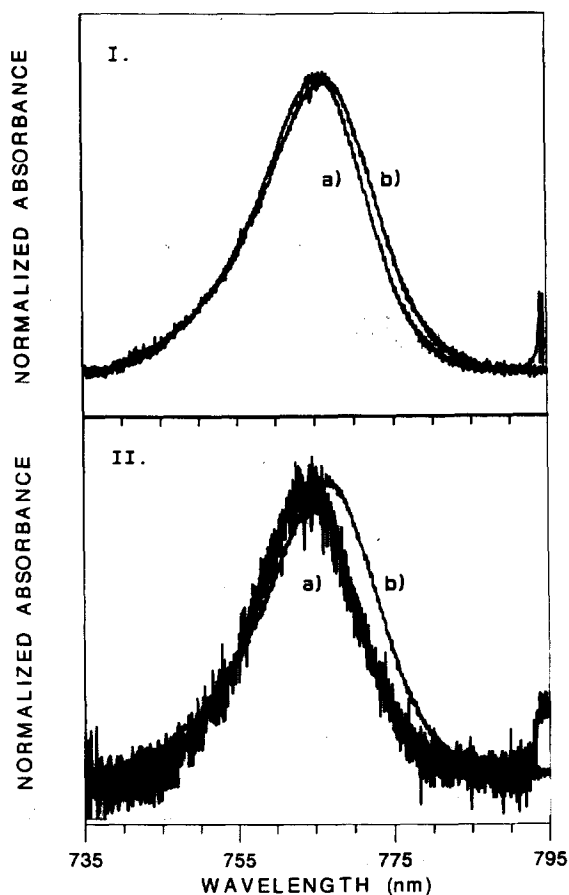
Fig. 2. Panel I shows an intensity normalized comparison of band III between fully photolyzed MbCO (b) and maximally photo-dissociated MbO$_2$ ($\approx$40% photolyzed) (a). The bottom shows the changes in the normalized band III for the oxy sample upon 80% recombination (a) of the 40% photolyzed sample ($\approx$8% photoproduct remaining) (b).

$\phi(t)$ defined as the [cw frequency at temperature T minus the frequency at high T (same as Mb)] divided by [the pulsed spectrum at T minus the high-temperature cw frequency]. Since the pulsed spectrum is of the completely photodissociated sample, it conveys primarily the temperature effect and not KHB or structural relaxation information. It can be seen that the temperature corrected frequency response starts above 130 K. The relative intensity however shows temperature corrected changes over a much broader region as can be inferred from figs. 7, 8 and 9.

Below $\approx$80 K the differences in the relative inten-
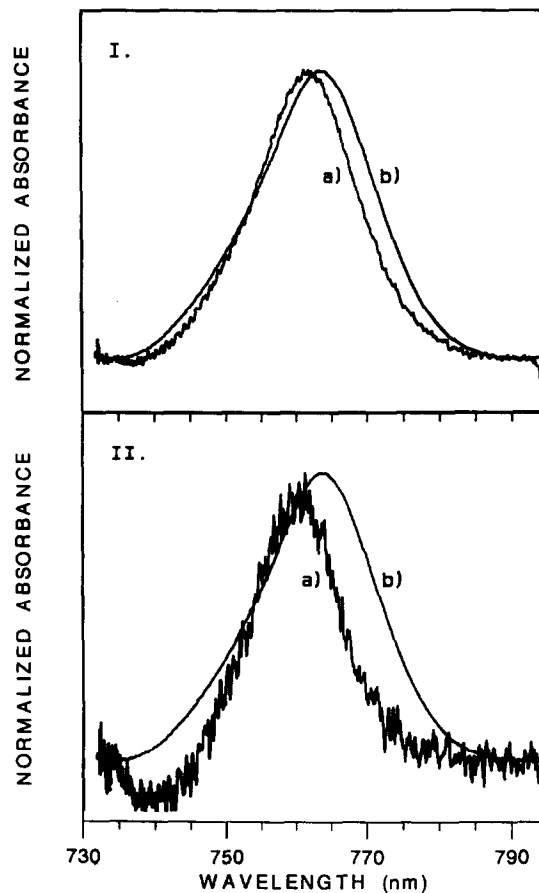
Fig. 3. Comparison of normalized band III for the photoproducts of the CO and O$_2$ derivatives of HbA (pH 6+IHP). Same comparisons as in fig. 2.

sity of the Fe–His band in the pulsed and cw spectra appears due to an optical pumping effect as seen in fig. 11. Fig. 11 shows how the relative intensity of ν(Fe–His) increases with illumination time for the pulsed excitation. The rate of spectral change with illumination becomes essentially imperceptible after about two minutes under these conditions. Furthermore, decreasing the pulse energy produces an end point spectrum with a lower relative intensity even after extended illumination. Similar changes are observed for the cw spectra but with the difference that for a given average power the end point cw spectrum has a lower relative intensity.

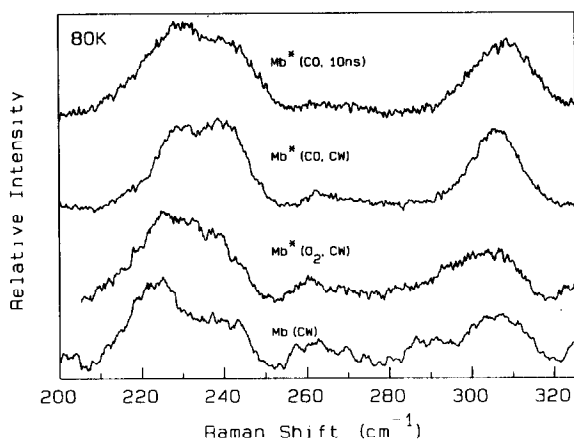Rousseau and co-workers [29] originally pointed out that the relative intensity of ν(Fe–His) at $\approx$4 K

Fig. 4. A comparison of the low-frequency region of the Raman spectra of equilibrium and nonequilibrium forms of five coordinate ferrous myglobin using cw and pulsed excitations at 442 nm. The peak at ≈ 232 cm^{-1} is the ν(Fe–His) mode. The bands at 240 and 310 cm^{-1} are derived from heme vibrations [24].

Fig. 6. Same series as in fig. 8 but using a pulsed excitation (10 ns, 50 Hz) at the same wavelength (442 nm) with roughly the same average power.
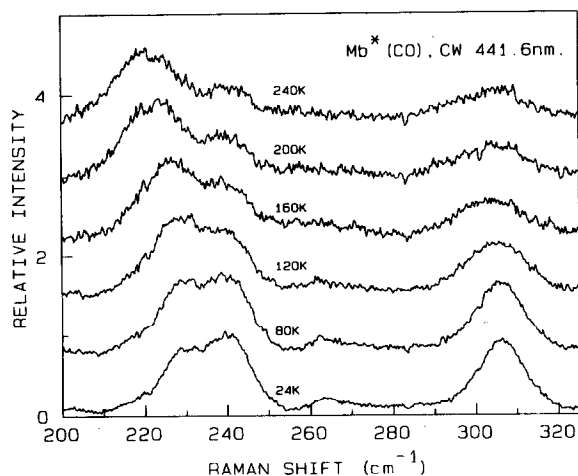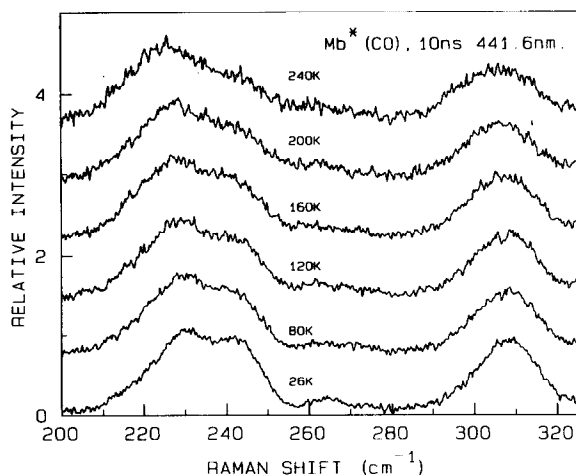

Fig. 5. A detailed view of the changes with increasing temperature in the low-frequency region of the cw (≈ 20 mW, 442 nm) Raman spectrum of Mb*(CO). The iron histidine stretching band is at ≈ 230 cm^{-1} over this temperature range. The intensities are normalized.

increases with increased cw laser intensity. We have continued to explore that phenomenon in an attempt to better understand its origin. Fig. 12 shows a comparison between a 2 K spectrum of Mb*(CO) that was cooled completely in the dark and the same 2 K sample after warming the sample to ≈ 5 K with the laser on and then returning back to 2 K after two

minutes. The major difference between the two is in the increase in relative intensity in ν(Fe–His) for the cycled sample. No such change is observed for a sample that is cycled in the dark even if the temperature is raised to as high as 80 K. The same basic effect is observed to occur at higher temperatures. By taking a series of one minute spectra over a several minute sequence at ≈ 5 K, we could see a rapid increase in the relative intensity of ν(Fe–His) similar to what we observe for the pulsed excitation. In a similar sequence at 25 K the same type of changes occurred but the total observed change in intensity is much smaller possibly because the major changes are over prior to the onset of our measurement. A larger effect of the same kind is observed when the same sample is cooled from 220 to 60 K with and without the laser illuminating the sample. The light cooled sample shows a higher relative intensity in the ν(Fe–His) than in the end point spectrum of the dark cooled sample. The same result was obtained upon multiple repetitions of the experiment.

The above optical pumping experiments help explain the spectral changes and differences observed in Mb*(CO) below ≈ 80 K. At these temperatures the sample is completely photodissociated. As the temperature increases the rate of ligand recombination increases which raises the issue of whether the spectral changes observed at higher temperature may
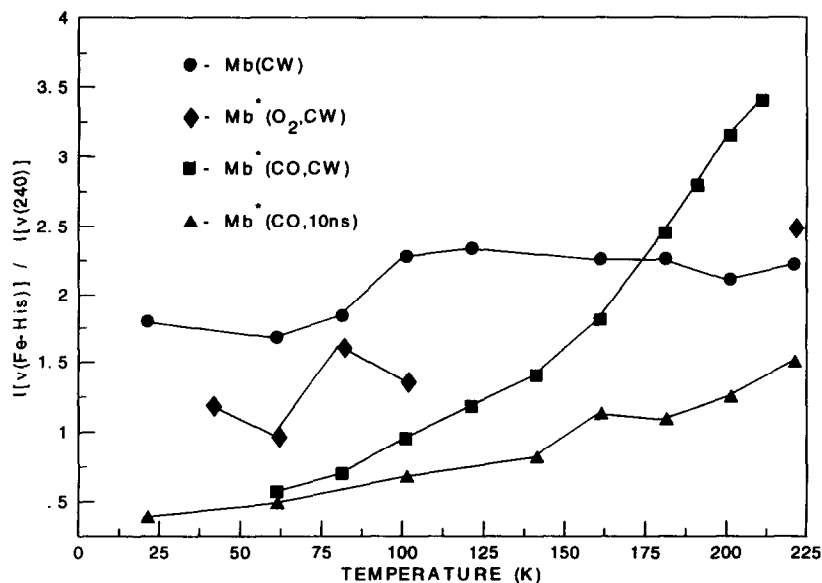
Fig. 7. The temperature dependence of the ratio of the intensities of ν(Fe–His) and the nearby heme associated mode at 240 cm^{-1} for different five coordinate forms of Mb. Intermediate points for the Mb*(O_2) were not obtainable due to the low yield of photoproduct at these temperatures. Large error bars are associated with the high-temperature values due to the difficulty in evaluating peak intensities in the presence of a large background. The data points for the pulsed excitation were obtained using a lower pulse energy than used for the spectra and data in the previous figures.
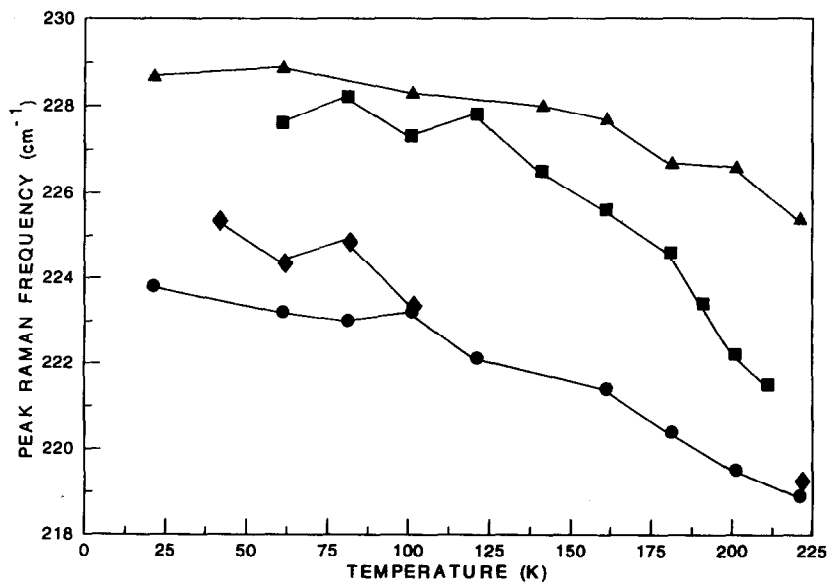
Fig. 8 The temperature dependence of the frequency of ν(Fe–His) for the same samples (same designations) as in fig. 7. The frequency changes for a given sample are more accurately determined than the intensity ratio.
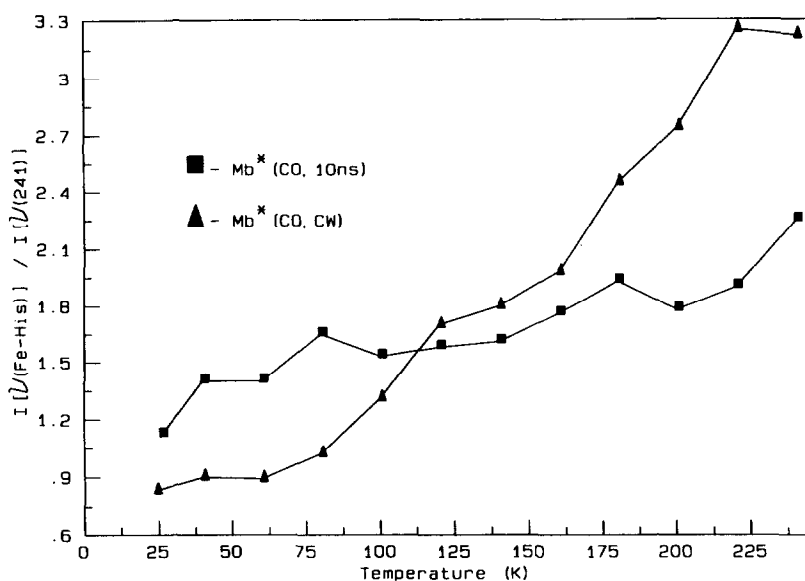
Fig. 9. A plot as a function of temperature of the relative intensity of ν(Fe–His) references against a heme Raman band at ≈ 240 cm^{-1} for the pulsed and cw spectra shown in figs. 5 and 6.
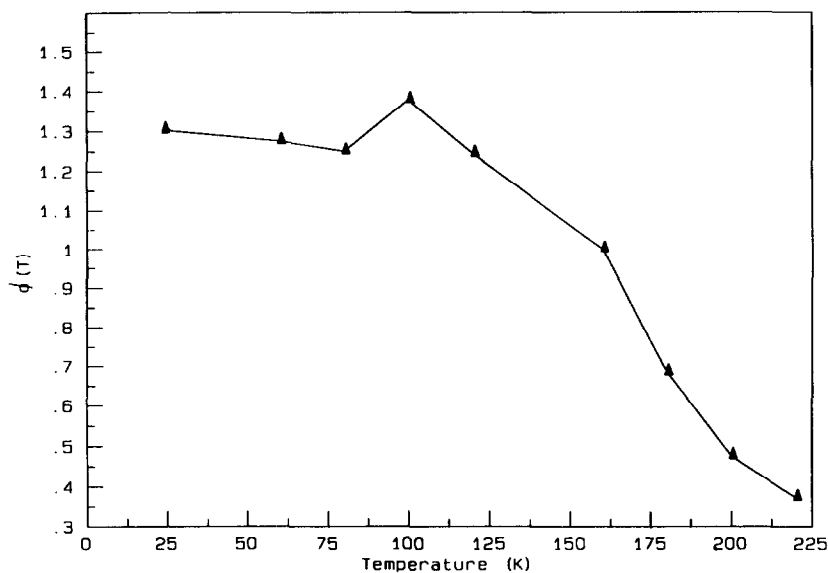
Fig. 10. A plot of the relaxation function for the frequency of ν(Fe–His) as a function of temperature. See text for details.

be due to KHB. This is an important issue since the corresponding oxy samples are both spectrally different from the CO samples and less photodissociated than the CO samples at all temperatures below 200 K as discussed below.

In the high-frequency region of the spectrum the ν_4 mode [24] can be used to monitor the relative amounts of photoproduct and ligand bound protein in the steady state created with the cw laser. Up through about 70 K there is little evidence of CO
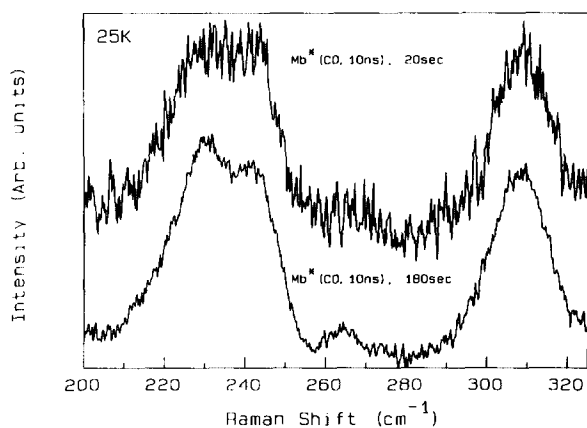
Fig. 11. The change in intensity of the low-frequency Raman spectrum of Mb*(CO) as a function of illumination time using the same pulsed excitation (excimer laser pumped dye laser) as used to generate the spectra in fig. 6. After 2 min the rate of change leveled off so that no further substantial changes were observed. The peak at ≈ 230 cm^{-1} is the ν(Fe–His) band.
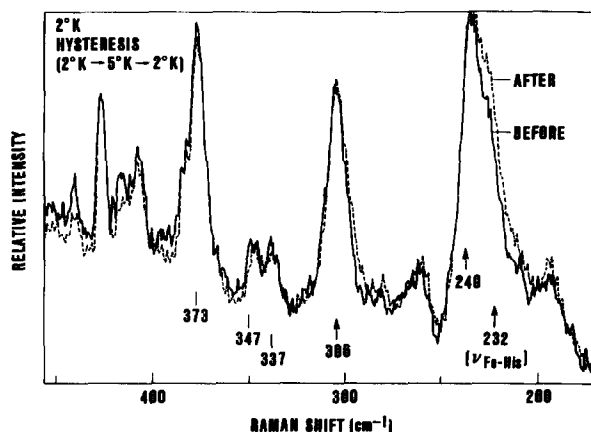
Fig. 12. Hysteresis effect on the 2 K cw Raman spectrum of Mb* upon illuminating the sample at 5 K for two minutes. Note the reversal in the energy axis compared to the privious spectra. At this temperature the ν(Fe–His) band is much lower in intensity relative to the adjacent 240 cm^{-1} band.

bound material present in the steady-state population. Above 70 K there is a progressive increase in the contribution from the six coordinate species. In the case of oxyMb there is a population of six coordinate heme present even at 2 K. At all temperatures the oxy sample exhibits a higher ratio of unphotolyzed to photolyzed material than that for the CO sample. At

or about 220 K there is a precipitous drop in the population of unphotolyzed oxyMb.

4. Discussion

4.1. An O_2 versus CO comparison: reactivity at cryogenic temperatures

The results obtained in this study are consistent with earlier observations that show:

(1) MbO_2 has a lower quantum yield of photolysis than MbCO [1].

(2) Whereas the entire population of conformational substates for MbCO is readily photodissociated at temperatures below ≈ 70 K, a substantial temperature dependent fraction of CS for MbO_2 can not be photodissociated even at liquid helium temperatures [15].

(3) The QY for the oxy derivative is distributed so that repetitive pumping does not alter the QY at liquid helium temperatures indicating that the QY is different for the different frozen noninterconverting CS [15].

(4) The population of MbO_2 that at cryogenic temperatures is photolyzable undergoes the same type of process I geminate recombination as the CO derived population [14,17].

These observations leave us with several unanswered questions which we address using the results of the present spectroscopic study. These questions include the following:

(1) What aspect of either electronic or nuclear structure produces the division of the MbO_2 sample into photolyzable and nonphotolyzable groupings at cryogenic temperatures. The inability to optically pump the nonphotolyzable population towards a higher total yield indicates that a simple branching ratio scheme involving excited electronic states [9,10] can not be operative unless the electronic state influences are strongly coupled to the distributed structural parameters of the conformational substates.

(2) Are the populations of the fully photolyzed MbCO sample and of the photodissociated part of the MbO_2 sample (which have similar distributions of barrier heights and preexponentials) comprised of the same distribution of conformational substates? In order to make any comparison between the two ligands

with respect to how protein structure influences reactivity it is necessary to be sure that one is comparing ligand rebinding reactivity within the same hemeprotein structure i.e. the same CS.

(3) Is the geminate recombination (process I) for both ligands controlled by the same structural elements?

(4) How does the protein select for O_2 over CO? At ambient temperatures the oxygen undergoes much more extensive geminate recombination than CO especially in Hb [11–13]. If both ligands undergo the geminate rebinding through the same process I (i.e. the same distribution of barrier heights and the same preexponentials) then the GR on the subnanosecond time scale, where ligand escape should be a minor factor, should be similar for the two ligands (but is not).

Our attempt to address these questions proceeds along the lines of first comparing the spectral properties of the photoproduct derived from both oxy and carboxy liganded bound proteins and then examining the behavior of the photoproduct spectra as a function of temperature. Varying the temperature allows for the creation of steady-state populations having varying amounts of photoproduct due to the temperature dependent changes in the recombination kinetics. Changes in the spectrum of the photoproduct that occur with changes in the relative populations of bound and dissociated protein provide a means of relating spectral features and hence structure to ligand reactivity through kinetic hole burning. Comparative KHB studies should provide indications as to whether similar structural controls of process I are operative for the two ligands.

4.2. Band III: a comparison of O_2 and CO derived photoproducts

Band III for Mb*(O_2) derived from a maximally photodissociated MbO$_2$ sample at liquid He temperatures resembles band III from the corresponding Mb*(CO) sample except that the former is missing the red edge of the latter. The Mb*(O_2) spectrum at 10 K and lower resembles an Mb*(CO) spectrum that has undergone substantial recombination. At these temperatures a maximally photodissociated MbO$_2$ sample is only $\approx 40\%$ dissociated whereas the CO sample is fully photolyzed [15]. Both photodisso-

ciated populations undergo minimal rebinding at these temperatures, i.e. those CS from either ligand bound species that have undergone photodissociation (on the 30 ps time scale) remain as photoproducts for time scales that are long compared to either the rate of photolysis using the cw laser ($\approx$ milliseconds) or the 10 Hz repetition rate used in earlier work [15]. With increasing temperatures the Mb*s from both ligand bound proteins begin to recombine. KHB is observed for both Mb*s. Increasing the extent of recombination results in both a decrease in the intensity of band III and a loss of the redder wavelengths in the band. Similar behavior is observed in Hb.

The band III results indicate the following:

(1) The mapping of the distribution of barrier heights for process I onto band III is similar for O_2 and CO [17].

(2) The structural element(s) responsible for the reactivity linked inhomogeneous broadening of band III is likely to be operating similarly in the control of process I for both ligands.

(3) Process I for Mb*(O_2) and Mb*(CO), although similar in terms of the kinetic parameters, involves two different distributions of CS. The population of CS that undergoes process I for Mb*(O_2) does not contain those CS that have for Mb*(CO) both the fastest recombination rates and the reddest wavelengths for band III.

(4) The missing red edge in band III for the maximally photolyzed MbO$_2$ sample < 10 K suggests that the CS population that corresponds to the missing red edge is also the CS population that can not be photodissociated (but would perhaps contribute to band III if they could be photodissociated with a short enough laser pulse). Alternatively the tertiary structural changes that are induced in Mb upon binding O_2 might not be as extensive as those engendered by the binding of CO and therefore the distribution of CS for Mb*(O_2) even for a fully photodissociated population might not contain those structural conformations that are the most shifted from that of Mb.

The band III studies clearly indicate the importance of deciphering the linkage between structure and spectra for the inhomogeneous distribution of CS that gives rise to the KHB phenomena associated with band III. The structures associated with the red edge of band III are derived both from CS that for Mb*(CO) represent those having the lowest barriers

for process I and from CS that for $Mb^*(O_2)$ are either nonphotolyzable (with 30 ps pulses) or are not accessible i.e. the binding of O_2 does not generate certain CS that are generated when CO binds. Although correlations between structure and wavelength have been inferred for band III based on the assignment of the transition giving rise to this absorption band (vide infra), a detailed picture of the structure is not readily derived from the absorption alone. To this end, the resonance Raman spectra of appropriate photoproducts are analyzed under conditions where correlations to band III behavior can be made. Since a number of temperature and laser induced changes can influence the Raman spectrum it is necessary to determine which processes are causing which changes in order to relate the spectral changes to well-characterized changes in either kinetics or absorption spectra.

4.3. Interpretation of Raman data

4.3.1. Between 2 and 40 K

At these temperatures the recombination rate of CO to Mb is sufficiently slow that the cw Raman spectra are reflective of a fully photodissociated population. As previously reported [24,29–31] the low-temperature Raman spectra of Mb^* display a ν(Fe–His) that is shifted to higher frequency and has a lower relative intensity than for Mb at the same temperature. The most evident change in the spectrum that occurs upon increasing the temperature is the progressive increase in the relative intensity of ν(Fe–His). There is no apparent change in the frequency over this temperature interval.

There are several possible origins for the observed increase in relative intensity with increasing temperature. Kinetic hole burning can be ruled out over this temperature interval since the CO sample appears to be fully photodissociated under these conditions and would therefore yield spectra that reflect the entire distribution of conformational substates. The other two most likely candidates are structural relaxation of Mb^* towards Mb and optical pumping in which repetitive photon excitation of Mb^* induces a structural change in the direction of Mb.

Structural relaxation is a plausible mechanism for the temperature dependent changes even at these low temperatures. Rousseau and co-workers suggested

[32] that the change in ν_2 for Mb^* in going from 4 to 40 K is due to structural relaxation involving the iron moving to a more out of plane configuration. It was also suggested [24,29–31] that the progressive increase in ν(Fe–His) over a similar temperature increment is due to a similar if not identical process. There are however several results that indicate that these spectral changes are not simply the result of an increased rate of simple structural relaxation of Mb^* towards Mb.

The hysteresis experiments show that the 2 K spectrum of Mb^* exhibits an increase in the relative intensity of ν(Fe–His) upon cycling the temperature up several degrees and back down to 2 K in the presence of ≈ 20 mW of cw laser radiation at 442 nm. No such change is observed when the temperature cycling occurs in the dark even when the temperature is cycled to much higher temperatures (5–70 K). We also find that at several temperatures above 2 K where the sample is fully photodissociated the intensity of ν(Fe–His) increases with irradiation time for both cw and pulsed excitations. Rousseau and co-workers showed that at 4 K the relative intensity of ν(Fe–His) increases with increased laser intensity [29]. Although our failing to obtain accurate beam sizes precludes a definitive statement, the more exaggerated pumping effects obtained with a 10 ns(50 Hz) excitation relative to a cw excitation of the same wavelength and average power suggests that turnover per unit time is more important than average power in effecting the light induced changes. These findings in the Raman spectrum mimic to a large degree the induced changes in the 760 nm absorption band in Mb^* observed by the Frauenfelder group [33]. These changes were interpreted as an optical pumping phenomenon where light acts as a catalyst for the observed relaxation towards a more Mb like spectrum. Increased illumination time, temperature and light intensity all increase the degree of relaxation of the 760 nm band. These results strongly indicate that the observed changes in the cw Raman spectrum of Mb^* (derived from MbCO) between 2 and ≈ 70 K are due primarily to optical pumping. This conclusion is further supported by the analysis from the Frauenfelder group [17] of the rebinding kinetics for photodissociated MbCO below 220 K which shows that the potential energy barrier controlling bond formation is much lower than that of the relaxed high-tempera-

ture species (> 220 K) and that the distribution of barrier heights does not change below ≈ 200 K unless the sample is optically pumped. Our KHB protocol [21,23] also indicates that there is no structural or spectral relaxation below ≈ 70 K in the weak illumination limit. When optically pumped the distribution shifts towards higher barriers consistent with the shift in band III towards a more deoxy like value [33]. Over this temperature interval where in the absence of optical pumping there is no change in the distribution of barrier heights, spectral changes (other than pure thermal effects) are not anticipated for functionally linked spectral bands. In particular we are referring to those spectral bands that reflect structural degrees of freedom that either are determinants of the barrier height controlling ligand rebinding or are somehow coupled to the distribution of barrier heights. Since the changes in ν(Fe–His) that are being discussed are directly linked to the control of the iron-ligand bond formation (vide infra), the attributing of the above changes in the Raman to optical pumping induced relaxation is entirely consistent with the full body of existing data regarding light induced spectral and kinetic changes in Mb* at cryogenic temperatures.

4.3.2. Above 100 K

The trend observed in the ν(Fe–His) of Mb* (from MbCO) upon raising the temperature from 2 to 60 K continues with increasing temperature. The relative intensity of this Raman band continues to increase until ≈ 200 K where the equilibrium value for Mb is approached. Between 100 and 180 K the increase in relative intensity of ν(Fe–His) with increasing temperature for the cw excitations appears to be enhanced over that which occurs over the lower temperature interval. Whereas below 100 K shifting of ν(Fe–His) is not observed with change in temperature, above 100 K decreases in frequency become more apparent with increasing temperatures. The trend of having more unphotolyzed species reflected in the Raman spectrum (ν_4) with increasing temperature is reversed above 180 K. The ν_4 region shows a predominantly five coordinate population at 220 K whereas at 160 K the six coordinate hemes dominate the steady-state population created by the cw excitation.

The changes in ν_4 occurring between 180 and 220

K in the Raman spectrum of Mb* are most consistent with a general loosening up of the protein that is associated with the glass-like transitions that have been characterized over this temperature regime [34]. Over these glass transitions occurs the onset of thermally driven protein structural fluctuations that result in interconversion among substates and ligand diffusion away from the narrow confines of the immediate heme environment and in structural relaxation (structural diffusion) towards the equilibrium Mb structure [17]. The sudden increase in the steady-state population of five coordinate heme photoproduct above 180 K is attributable either to the increased probability of ligand escape upon photolysis (the solvent process in the language of the Frauenfelder group) or to the increased barrier height for bond reformation due the rapid relaxation of Mb* to Mb on the time scale of recombination.

4.3.3. Structural diffusion

The Frauenfelder group [2,35,36] initially interpreted the qualitative change in recombination kinetics at the glass transition as being due to the onset of a matrix process where the ligand recombines from the bulk protein rather than the heme pocket. For both process I (recombination from that region of the distal heme pocket that is proximate to the iron in which the photodissociated ligand is localized either at temperatures below the glass transition or at very short time intervals following photodissociation) and the matrix process the same distribution of barrier heights for bond formation was assumed and used. Subsequently, Agmon and Hopfield [37] in their analysis of the MbCO recombination kinetics, concluded that the slow down in recombination around 200 K could be due to structural diffusion of the Mb* structure to the Mb structure with its associated higher distribution of barrier heights. If upon photodissociation the structural degrees of freedom that control the barrier height for rebinding relax to a higher barrier configuration (e.g. Mb*→Mb) on a time scale that is comparable to or faster than the rebinding times, then the distribution of barrier heights will be influenced or determined by the relaxed structure and not the instantaneous photoproduct structure. At the same time that Agmon and Hopfield came out with the AH model of structural diffusion and reactivity, Friedman and co-workers [38,27] using time resolved res-

onance Raman found evidence for such an effect in hemoglobins. The iron proximal histidine linkage shows clear changes over a wide range of time scales that includes the 100 ns window during which geminate recombination occurs. Since the frequency shifts in ν(Fe–His) are linked to the barrier controlling the bond forming step in the geminate process [13,27], it was concluded that as this structural relaxation took place the barrier should be increasing. Whereas the iron proximal histidine linkage in Hb* relaxes over a time course that spans nanoseconds to tens of microseconds [38,39,40], Mb* at 30 ps exhibits a ν(Fe–His) that is essentially identical to that of Mb [41]. This observation made it difficult to accept the notion that the recombination of CO to Mb* below 180 K, where Mb* has a very different ν(Fe–His) from Mb, could be describable in terms of the same distribution of barrier heights (for process I) as for ambient temperatures where Mb* reverts to Mb faster than any observed process I recombination [40]. The recent reanalysis of the kinetic data by the Frauenfelder group [17] clearly shows the slow down in process I at the glass transition without the need to invoke a matrix process.

4.3.4. Kinetic hole burning

The changes that occur in the cw Raman spectrum of Mb* between 2 and ≈ 70 K are uncomplicated by the presence of a substantial population of ligand bound protein. The observed changes are interpreted as arising primarily from an optical pumping process that facilitates the relaxation of Mb* towards Mb. Above ≈ 100 K the increased rate of recombination complicates the interpretation of the temperature dependent spectral changes. We focus on the temperature regime below 180 K since the changes occurring above 180 K can be additionally complicated by the onset of large scale fluctuation as discussed in the previous subsection.

There are four possible sources for the observed temperature dependent spectral changes:

(1) Pure thermal effects such as changes in structure due to thermal expansion and changes in vibrational populations.

(2) Optical pumping induced relaxation of Mb*.

(3) Spontaneous relaxation of Mb*.

(4) Kinetic hole burning due to ligand recombination.

The observation that over this temperature range the spectra of Mb* when generated with a 10 ns laser pulse (complete photolysis) do not show the changes observed for the cw spectra indicates that at least some significant fraction of the effect is not due to a pure thermal effect. The 10 ns photoproduct spectrum differs from the cw spectrum in that the former contains contributions from a much larger population of photoproduct. The cw steady-state population reflects those conformational substates that are slowest to recombine relative to the photolysis rate of the excitation. The 10 ns spectrum of Mb* has contributions from fast and slow recombining substates. The fact that the 10 ns spectrum at 160 K resembles a cw spectrum taken at a lower temperature where the steady-state population contains more photoproduct than at the higher temperature is consistent with either a relaxation process or a kinetic hole burning process being responsible for at least some of the changes in ν(Fe–His) that occur with increasing temperature above 100 K.

Two key observations indicate that it is KHB and not structural relaxation (diffusion) that is responsible for the 100 to 180 K spectral changes in ν(Fe–His):

(1) Our observation that in comparing different samples under different excitation conditions the more unphotolyzed material evident in the spectrum, the more exaggerated are the differences between that spectrum and the spectrum of the more fully photodissociated sample obtained below 70 K. Those cw spectra that reflect a substantial amount of recombination occurring on a time scale comparable to the rate of photolysis always have a ν(Fe–His) that has Mb-like features, i.e. a high relative intensity and a reduced frequency.

(2) The analysis of the Frauenfelder group [17] indicating an absence of spontaneous relaxation of protein structure below 180 K, derived from the observation that the same distribution of barrier heights can account for the recombination process from 40 to 180 K.

Number two indicates that spontaneous relaxation of those structural degrees of freedom in Mb* that control the distribution of barrier heights for process I does not begin below ≈ 180 K. To the extent that the structure reflected in ν(Fe–His) is correlated with the process I barriers (vide infra), spontaneous re-

laxation of the iron–proximal histidine linkage below 180 K is not consistent with observation 2; however, the possibility that laser induced relaxation is responsible for all or most of the below 180 K temperature effects is not ruled out. Observation 1 does argue against either spontaneous or laser induced structural relaxation being responsible for the temperature correlated spectral changes since both sould be more apparent in samples that have the least amount of unphotolyzed material. Relaxation of Mb*, either spontaneous or photon assisted, is favored by the creation of the five coordinate photoproduct. Thus at a given temperature those steady-state sample conditions favoring enhanced photolysis should yield the most relaxed looking spectra but they do not. Instead, the most relaxed looking spectra come from those samples having the least amount of photoproduct as is especially evident in comparisons between oxy and carbon monoxy myoglobin at the same concentration and temperature (vide infra). The former shows much less photoproduct at any given temperature and yet in comparison to the more fully photodissociated MbCO sample the spectrum looks far more relaxed. Overall the interpretation of the temperature correlated changes in ν(Fe–His) is most consistent with KHB being responsible for the most evident changes occurring between 100 and 180 K.

4.4. Correlations between the Raman spectrum and band III

Earlier studies show a similarity in the behavior of band III and ν(Fe–His) [23,40]. The present study extends the earlier comparisons to the more subtle changes that occur at cryogenic temperatures as a result of KHB, optical pumping and relaxation.

4.4.1. Optical pumping

Frauenfelder and co-workers showed that the slowing down of the ligand recombination kinetics upon extended illumination of Mb* at temperatures below 100 K is associated with a shift in band III to bluer wavelengths for the fully photodissociated sample of MbCO [33]. In the absence of extended or intense illumination there is no shifting of band III for the *fully* photolyzed sample [21,33]. The relationship between the wavelength of band III and the barrier height for process I is found to hold for the optically

pumped sample [33], i.e. the new distribution of barrier heights of the optically pumped sample maps onto the wavelengths of the shifted band III.

The changes in the Raman spectrum of Mb* upon optical pumping are distinct. At temperatures where ligand rebinding is insignificant and hence KHB is not a factor, by far the most prominent change is an increase in the relative intensity of ν(Fe–His) with increased illumination of Mb*. The absence of the hysteresis effect for the 2 K Mb* spectrum when the sample is warmed (from 4 to 70 K) in the dark indicates that the changes are not due to spontaneous relaxation. Below 70 K there is no detectable shifting of the frequency of ν(Fe–His) only relative intensity changes. Thus the blue shifting of band III upon optical pumping appears to correlate with increases in the relative intensity of ν(Fe–His).

4.4.2. Kinetic hole burning

KHB in both Mb* and Hb* is characterized by a progressive loss of the red edge of band III with increasing amounts of ligand recombination. The Raman spectrum of Mb* show changes with increasing temperature that are attributable to KHB. The changes are primarily an increase in the relative intensity and a decrease in frequency of ν(Fe–His) with increasing amounts of ligand recombination. For steady-state populations that show high levels of recombination, there are indications that the remaining Mb* have a ν(Fe–His) that has not only a very high relative intensity but also a frequency that is shifted towards Mb relative to the maximally photodissociated sample. The present study shows that at least in Mb the wavelength of band III correlates with not only the frequency of ν(Fe–His) but also its relative intensity. The fastest recombining CS of the Mb*(CO) population are those that have the reddest band IIIs and the most intense and highest frequency ν(Fe–His). The results suggest that for Mb* the majority of the CS have a relatively narrow distribution of ν(Fe–His) frequencies which are $\approx 10\ \mathrm{cm}^{-1}$ higher than the peak frequency of Mb. Within this relatively narrow distribution of high-frequency CSs there is a large distribution of CS that have ν(Fe–His)s of similar frequency but different relative intensities. Within this grouping, those CS with the ν(Fe–His) having the lowest relative intensity are those with the lowest barrier for process I. The slowest rebinding CS are

those that have the bluest band III and the most deoxy Mb like ν(Fe–His), i.e. low frequency and high relative intensity.

4.4.3. Correlations between the Raman and other induced spectral changes

Champion and co-workers found that illuminating an MbCO sample while cooling the sample from above the ≈ 180 K glass transition, where relaxation can occur, to below 60 K where the structures are essentially frozen, produced Mb* species that have a more deoxy like Soret absorption band [42]. If the starting temperature is below the glass transition the shift is dramatically reduced or eliminated. The idea behind this experiment which was suggested by Agmon and Hopfield [37] is that if upon going from above to below the glass transition the ligand can on average be kept off the heme long enough to allow for relaxation of Mb* to or towards Mb, then a partially or fully relaxed Mb* can be trapped at cryogenic temperatures. If the ligand is not trapped outside the heme pocket (or proximate location where process I recombination can occur) during the cooling process then the kinetics for process I should be much slower due to the more relaxed Mb* structure. A shift in the distribution of barrier heights to higher values does appear to occur under the above cooling protocol based on the Raman data. The effect is much larger than the optical pumping effect which does not include a cooling step from above the glass transition. In the present study, it is found that cooling MbCO under laser illumination (much lower intensity than in the Champion study) from 220 to 60 K produces an Mb* spectrum with a higher relative intensity ν(Fe–His) than for the same sample cooled at the same rate but in the dark. The results suggest that the structural parameter associated with variation in the relative intensity of ν(Fe–His) for Mb* is connected with differences in the properties between Mb and Mb*.

4.5. Spectra and structure

The band III and Raman studies together suggest that there is a hierarchy of conformational substates [17,34–36] associated with the coupled iron and proximal heme environments for Mb* and Mb. The data is consistent with there being two tiers of struc-

ture associated with the proximal heme pocket. First there is a population of CS separated by barriers that are sufficiently large that interconversion or relaxation processes among these CS does not occur until near or at the glass transition. These CS are characterized by different frequencies for ν(Fe–His). For Mb* below 180 K this population of CS is skewed towards the highest frequency, whereas for Mb the low-frequency CS are favored. The next tier of CS has lower barriers separating the conformations as reflected in the optical pumping experiments. This tier is made up of CS that have different relative intensities associated with ν(Fe–His). For this tier the most relaxed CS (most Mb-like) are those CS with the highest relative intensity for ν(Fe–His). Studies on a fish hemoglobin with an exceptionally low ligand affinity in which the second tier CS behave like those of Mb (with respect to Mb*–Mb differences) show that the two tiers are not obligatorily coupled [27]. The cw laser intensities used in our study (< 30 mW) induced detectable optical pumping within this tier of CS but not the first tier as reflected in the progressive increase in relative intensity of ν(Fe–His) without a concomitant shift in frequency. The Raman data suggest that even for a relatively narrow distribution of the hard to interconvert CS (i.e. a narrow distribution of frequencies for ν(Fe–His)) there can be a relatively large distribution of the easier to interconvert CS (tier two) resulting in a wide distribution of relative intensities. The KHB results indicate that the two tiers may be correlated in that the low relative intensity second tier CS and the high-frequency first tier CS recombine first. Whereas the changes in relative intensity of ν(Fe–His) are evident at the lowest levels of recombination, shifts in the frequency of ν(Fe–His) are not apparent until the steady-state population contains a substantially reduced fraction of photoproduct. The KHB conclusions from the Raman spectra indicate that it is the CS from the second tier that are the principle participants in several phenomena involving band III. These phenomena include:

(1) The loss of the red edge of band III in the earliest stages of KHB for Mb*.

(2) The shifting of band III to the blue upon low levels of optical pumping.

(3) Some of the red edge difference between

$Mb^*(O_2)$ and $Mb^*(CO)$ at liquid helium temperatures.

Previous studies of ν(Fe–His) suggest plausible assignments for the structural degrees of freedom that vary within each of the above discussed tiers of CS. The first tier is associated with CS that have different frequencies for ν(Fe–His). For Mb and Hb, such frequency differences are attributed to alterations in the iron–histidine bond strength due to changes in the tilt angle θ between the heme and the proximal histidine [24–27]. The higher-frequency conformations are those with the less tilted structures. Changes in this degree of freedom are linked to global tertiary structure changes [43].

Variation in the relative intensity of the ν(Fe–His) is attributed [27,28] to variations in the azimuthal angle of the proximal imidazole with respect to the iron pyrrole nitrogen axis. An eclipsing orientation is associated with the highest relative intensity due to a maximum overlap of π electron orbitals from the heme and the imidazole which creates the maximum Soret band resonance enhancement for ν(Fe–His) [27]. Moving from an eclipsing conformation to one that is off axis results in a decrease in relative intensity of ν(Fe–His) due to a decrease in π overlap with the accompanying drop in resonance enhancement. Thus the second tier consists of CS with differing azimuthal angles ϕ. Within the hierarchical Frauenfelder model of the CS [35], each of the first tier CS (corresponding to a specific tilt of the heme–histidine unit) has an associated set of second tier CS

It is reasonable that changes in the wavelength of band III can be due to changes in either tier of proximal substates. The large wavelength changes in band III in going from either Mb* to Mb or Hb* to Hb are noticeably connected to the first tier of proximal CS, whereas the KHB and optical pumping induces changes in Mb* are to a large measure due to changes in the population of contributing second tier CS at least in myoglobin.

It is not surprising that population changes in either tier can influence the wavelength of band III based on the currently accepted assignment for band III [20] in which an electron from the highest filled π orbitals of the porphyrin is promoted to a half filled d_{xz} or d_{yz} orbital of the iron. Variation in the energy of that iron d orbital as a function of iron displacement can been viewed as the likely origin of the

wavelength dependence of band III [22]. Empirically, smaller displacements are linked to a reduced interaction given rise to a red shifted band III. In addressing not only the current issue but also issues pertaining to how structure controls reactivity, the fundamental question is now centered on whether the iron displacement is determined by factors other than those related to the proximal parameters or whether the proximal parameters in fact dictate the iron displacement (as well as the orbital interaction). If the iron moves out of the heme plane upon photolysis because the high spin ferrous iron cannot fit into the heme plane then the proximal parameters are at best a secondary influence on the iron coordinate and reactivity. On the other hand, calculations [44] show that the heme core can accommodate a high spin ferrous iron (quintet state). The calculations indicate that it is the repulsive interaction between the fifth ligand (the proximal histidine) and the heme that causes the iron to move out of plane. The mixing of the repulsive potential with that of the quintet state is what produces an equilibrium position that is nonplanar. Since in this picture it is the proximal parameters that are the determinants of both the repulsive part of the potential and the iron displacement, all of the spectral and structural elements under discussion are intimately coupled. Elements of this model have been discussed in detail in an earlier paper [27].

4.6. Mb*: structure and dynamics

Below 180 K, Mb* differs from Mb in having a red shifted and broader band III and a higher frequency but lower intensity ν(Fe–His). The above analysis indicates that in relation to Mb, Mb* has a less tilted heme–histidine unit, a broader distribution of second tier CS, and a distribution of second tier CS that is skewed towards larger values of ϕ.

The above analysis also suggests a relaxation pathway for Mb*. The movement of the iron into the heme plane upon ligand binding results in tertiary structure changes that are likely to involve the movement or sliding of α helices (based on the changes in tier 1 parameters in going from Mb to Mb*). The tertiary structure changes are driven by an enhancement of the repulsive interaction between the heme and the proximal histidine upon moving the iron to a more planar position upon ligand binding. The enhance-

ment of the repulsive interaction as the iron moves in-plane for Mb, forces the histidine to assume a less tilted orientation [26,39] which initiates the shift in the helices. Resumption of the initial tilted orientation (associated with Mb) upon ligand dissociation requires movement (sliding) of the helices in Mb* subsequent to photodissociation. The structure of Mb and ligand bound myoglobin is distinctly different. Subsequent to photodissociation the structure of Mb* is initially related to that of the ligand bound form. Reorganization of the protein structure is required to relax back to the equilibrium Mb configuration. At room temperatures the structure and its environment are sufficiently mobile that relaxation of Mb* to Mb is largely complete within 30 ps [41]. Below the glass transition the global fluctuations of the protein are frozen out and reorganization of aspects of the protein structure is limited or bound by the overall conformation of the protein that was frozen upon cooling below the glass transition. As a result a population of Mb* can be trapped that has the initial tertiary structure of the liganded globin. Starting at 2 K, the following sequence of events subsequent to photodissociation is envisioned. Prior to photolysis the sample exists as a frozen distribution of tertiary structures each having the iron in some position close to or in the plane of the heme. Within picoseconds or less of photolysis, the iron in each of the frozen CS moves in response to the unbalanced repulsive interaction that stems from the proximal parameters determined by the specific tertiary structure of the CS. The final displacement of the iron in a given CS at this temperature is uniquely determined by the proximal parameters of the given CS. Thus for each frozen CS (tertiary structure of the globin) there are at least two well defined positions of the iron: one associated with the ligand bound species and one with the five coordinate photoproduct. Additional relaxation to the extent that it occurs (primarily optical pumping) involves the second tier of CS at least below 100 K. We envision the relaxation as a corkscrew type motion where the irons from the most in-plane CS, which are the ones with the largest values of ϕ, move further out of the heme plane as the imidazole ring undergoes a corkscrew type motion towards the lower values of ϕ that are seemingly favored by the proximal heme pocket. The shifting of the distribution of the second tier CS towards larger values of ϕ

in Mb* probably reflects a means of reducing the increase in the repulsive interaction between the heme and the histidine when the iron moves in-plane in response to ligand binding.

4.7. Structure and reactivity

There is a large body of experimental and theoretical data indicating that in general the binding of a ligand to a five coordinate high spin ferrous heme is accompanied by the movement of the iron from an out-of-plane position to a more in-plane position. We wish to consider how this observation in conjunction with the structural insights from this study impact on our understanding of how the protein structure controls ligand binding including how the protein discriminates between oxygen and carbon monoxide.

4.7.1. Proximal control of reactivity

If we assume that ligand–iron bond formation can occur only when the ligand and heme are closely spaced (proximate geminate pair, encounter complex), then there are two limiting cases for the process of going from the encounter complex to the heme-bound ligand:

(1) The ligand forms a weak bond with the out-of-plane iron which then moves to the more stable in-plane configuration having a stronger iron–ligand bond. Once the encounter pair is formed, there is little or no barrier for bond formation since the steps leading to the stable in-plane configuration are all energetically down hill.

(2) The ligand can only form a bond from within the encounter complex when the iron is either in-plane or less out-of-plane compared to the average displacement associated with the starting heme species. In this case the barrier for bond formation is related to the probability that during the lifetime of the encounter complex, the heme undergoes a fluctuation that creates a transient planar structure that exists long enough for the bond to form.

We now consider how the proximal parameters influence the bond forming process in each of the two limiting cases. As discussed earlier, the out-of-plane displacement of the iron is caused by the introduction of a repulsive potential by the nonbonded interactions of the proximal histidine with the heme. Both a decrease in the frequency and an increase in rela-

tive intensity of ν(Fe–His) signifies an increase in the repulsive interaction. This increase has the effect of favoring a more out-of-plane configuration for the five coordinate species and of making it energetically costly to move the iron to an in-plane position. As a first approximation the potential surface that determines the energetics of the iron can be viewed as a harmonic potential [28,37], where the tertiary structure of a given substate determines both the spring constant and the iron displacement. In this model, the spectral parameters associated with ν(Fe–His) are a reflection of the proximal contribution to the spring constant [13,24–27]. An increase in the repulsive interaction, as reflected in either a decrease in the frequency or an increase in the relative intensity of ν(Fe–His) indicates an increase in the spring constant. Thus for a distribution of CS, there is a distribution of proximal parameters each of which defines a proximal contribution to the spring constant. Furthermore, each of these CS with its specific spring constant determines a specific mean displacement for the five coordinate form of the CS. Each frozen CS has a unique range of accessible displacements which are a function of ligation state and temperature. For a given ligation state of a specific CS, both the most probable displacement distance and the range of fluctuation driven excursions of the iron from that position are functions of the proximal parameters within this model. We emphasize that each CS in the second tier (well defined tilt and azimuthal angles for the proximal histidine) has its own set of displacement and fluctuation parameters.

In the first case where the ligand binds to the out-of-plane iron, bond formation can be influenced by the proximal parameters in two ways: the rate of spontaneous dissociation of the meta-stable and stable bound forms and possibly the rate at which the stable bond forms from the encounter complex once the meta-stable bond is formed (where the meta-stable bond refers to the bond that is formed prior to any movement of the iron towards the heme plane). Both of these influences stem from the stability of the bond decreasing with the increasing displacement of the iron from the heme plane. Since there is no proximal contribution to variations in the energetics of the formation of the initial meta-stable bond (since there is no initial movement of the iron) the energy of the transition state is going to be relatively insen-

sitive to variations in the proximal parameters. The magnitude of the subsequent drop in energy as the six coordinate iron moves in-plane will depend upon the proximal parameters as a result of the work done against the spring. The insensitivity to the proximal parameters of the transition state energies relative to the stability of the final bond (after iron movement) leads to the spontaneous dissociation rate being modulated by proximal interactions. Those CS with proximal parameters that strongly favor a displaced iron will have a five coordinate structure with a large iron displacement and a ligand bound structure that has an iron–ligand bond that is destabilized by the amount of work necessary to move the iron in-plane. The latter favors an increase in the dissociation rate.

In the second case for bond formation, there is an added influence of the proximal parameters. This added influence is due to the requirement that to form a bond, the iron must be in a more in-plane position than the mean displacement associated with the five coordinate form of the CS in question. Thus bond formation proceeds through fluctuation driven motions of the iron that transiently take it to a position where bond formation can occur. The rate controlling the bond forming process should therefore be dependent upon the equilibrium fluctuations of the specific CS which includes the cost in energy of moving the iron to the more in-plane position while it is still five coordinate. Once the bond is formed the system can self-trap as described above. The proximal contribution to the barrier height controlling bond formation would therefore be related to the energy necessary to move the iron to the more in-plane position prior to binding. Since within this model the binding occurs only during the time interval when a transient intermediate exists, the binding rate must be related to the probability that the needed displacement occurs within some time window such as the lifetime of the encounter complex. If at a given temperature the fluctuation spectrum is such that there is a very high probability of finding the iron at the required position (i.e. the energy separation between the mean displacement and the shifted displacement is less than kT), then the binding from the encounter complex should appear barrierless. The proximal parameters influence the barrier height by modulating the energy separation between the five coordinate transition state form of a CS and the initial five co-

ordinate form of the CS. For example a second tier CS having a blue shifted band III and a low frequency–high relative intensity ν(Fe–His) should have an encounter complex with a maximally displaced iron. This CS would therefore have a larger barrier than for a CS having a less "repulsive" set of proximal parameters. If the proximal parameters are sufficiently less repulsive i.e. a very red band III and a high frequency ν(Fe–His), then the iron is only slightly displaced and there is only a small energy gap separating the starting and transition state forms of the five coordinate CS. As a consequence the onset of zero barrier binding for this CS should occur at much lower temperatures than for the previous CS.

4.7.2. A comparison of Mb*(O₂) and Mb*(CO)

At liquid helium temperatures there are distinct differences in the spectra of Mb*(O$_2$) and Mb*(CO). Most obvious are the difference in intensities due to not being able to photodissociate more than $\approx 40\%$ of the MbO$_2$ sample in contrast to the fully photodissociated MbCO sample. Process I for both samples at these temperatures is essentially nonexistent compared to the rate of photolysis. In comparing the photoproduct spectra, we see that relative to Mb*(CO), Mb*(O$_2$) has a band III that is missing the red edge and a ν(Fe–His) that has a higher relative intensity and a slightly lower frequency. These observations indicate that the distribution of CS that comprise the photodissociated population of the MbO$_2$ sample is different than that of MbCO. The former has a CS photoproduct population that is missing those CS that represent the CS found in Mb*(CO) that have the least repulsive proximal parameters. With increasing temperatures both samples show increases in the steady-state population of ligand bound protein. For CO which has a near unity QY of photolysis, the increased presence in the cw spectra of CO bound protein signifies an increase in the rate of process I. For O$_2$, the increase is also due to a progressive decrease in the QY with increasing temperatures as well as the increased rate of process I. At any given temperature below 180 K the O$_2$ sample displays significantly less photoproduct than the corresponding CO sample. Both samples show similar KHB effects both in band III and in ν(Fe–His) with increasing temperatures. In every instance at a given temperature the O$_2$ sample displays a photoproduct spectrum that appears

more "hole burned" than the corresponding CO sample and therefore looks more relaxed (vide supra). The overall pattern suggests that at liquid helium temperatures the O$_2$–CO differences arise from KHB in the O$_2$ sample due the population of unphotolyzable CS. The alternative explanation, that the binding of O$_2$ fails to generate those missing CS, makes it rather difficult to explain why the QY appears distributed (cannot be increased with extended or repetitive pulsing even at 4 K) [15]. We will therefore proceed on the assumption that the missing CS are associated with the nonphotolyzable part of the CS population and that the low QY is due to ultrafast ($\ll 30$ ps) recombination as implied from femtosecond studies. We are left with the task of understanding why those CS that for CO have the fastest rates for barrier controlled process I, undergo what appears to be an ultrafast barrierless recombination for O$_2$. The "red edge" CS in question have proximal parameters that indicate a reduced repulsive interaction which is associated with a reduced spring constant and a small iron displacement.

In an earlier paper we noted [15] that O$_2$ but not CO appears able to form a stable bond with a nonplanar iron. Theoretical calculations support that conclusion. Whereas CO can only form a stable bond with the singlet state of the ferrous iron (low spin), calculations by Goddard and Olafson [44] show that for O$_2$ the most stable bond is formed with the triplet state (intermediate spin) iron. Other calculations by Karplus [45] indicate that both the triplet and singlet contribute to the formation of the iron–oxygen bond. Goddard also shows that O$_2$ can form a stable albeit weaker bond with the quintet state (high spin). The important point about the theoretical calculations is that the combination of the electronic potentials with the repulsive potential of the fifth ligand results in the minima of the three spin states being shifted to differing degrees along the iron displacement axis. The quintet state is the most stable at large iron displacements. The energy separation between the three states decreases as the iron moves closer in-plane with the triplet being closer to the quintet. The greater the repulsive interaction, i.e. the steeper the potential, the greater is the energy separation among the states. For a shallow repulsive potential of the kind one might expect for the red edge CS, the iron is slightly displaced in the five coordinate species. Un-

der these conditions the quintet and the triplet can be rather close in energy. Since oxygen can bind to the triplet, there should be iron displacements for which bond formation can occur without a barrier. For CO, however the requirement that the bond forming state be the singlet necessitates the motion of the iron further in-plane in order to access the singlet. This requirement means that the transition state for the CO will be destabilized relative to that of initial five coordinates CS resulting in a proximal contribution to the barrier for bond formation. Thus for these "red edge" CS the formation of the iron ligand bond falls into case (1), and case (2) for O_2 and CO, respectively. These arguments are reminiscent of conclusions by Szabo [46] regarding the nature of the transition states for the two ligands. Szabo derived his conclusion from the relative sensitivity of the on and off rates to protein structure for the two ligands.

The above analysis suggests that under certain circumstances CO can behave like O_2. The binding of CO should revert to the barrierless limit for those CS where the iron is essentially in-plane. Agmon and Hopfield predicted such an effect [37]. Such behavior has been observed for cryogenically trapped MbCO at pH = 3 where a large fraction of the sample cannot be photodissociated with a 30 ps laser and process I occurs over a time scale that starts with picoseconds [47,48]. The switch for CO in this instance is explained [47] in terms of a protonation induced lengthening and weakening of the Fe–His bond that creates a population of photoproducts with nearly in-plane iron.

Increasing the temperature from 4 K results in an increase in the fraction of "nonphotolyzable" MbO_2 as well as an increase in the rates of process I for both CO and O_2. There have been other explanations for the origin of the low QY for O_2 at cryogenic temperatures. Frauenfelder and co-workers [17] have put forth a reasonable explanation based on what they call process I*. The ultrafast recombination is claimed to be due to rebinding to those CS that have not undergone the full iron relaxation commensurate with the particular substate. Since at these cryogenic temperatures the iron has not relaxed for some fraction of the population of CS, fast recombination can occur. If the ultrafast population is derived from unrelaxed CS, then as the temperature increases the yield of un-

relaxed CS should decrease and the QY should increase which is contrary to what is observed. Even if one postulates different relaxation rates for the different CS with the "red edge" CS relaxing the slowest in order to account for the absence of a detectable pumping effect for the QY, there should still be a decrease in the fraction nonphotolyzable CS with increasing temperatures if the process depends on the relaxation rate of the iron subsequent to photodissociation. Alternatively the correct temperature dependence is obtained from the assumptions that all the CS undergo relaxation upon photodissociation, that different CS have different mean displacements of the iron for the photoproduct, that at any given temperature there is a group of CS that have the iron sufficiently in-plane for barrierless recombination and that as a result of the increase in the amplitude and frequency of the thermally driven fluctuations of the iron displacement coordinate with increasing temperatures the number of CS that fall within the barrierless group increases.

The model presented above also predicts that other recombination processes should appear in addition to process I. For the O_2 ligand at some intermediate temperature between 4 K and the glass transition there will be a fraction of the Mb* CS that undergo ultrafast barrierless recombination, a fraction (the bluer band III CS) that undergoes recombination via process I since motion of the iron is required to form the transition state, and a fraction in a gray zone with a fluctuation spectrum that contains occasional jumps in the iron position which allows barrierless recombination to occur. If on the time scale of the fastest decade of process I there is no interconversion of substates, then as long as the depletion of the gray zone population of Mb* via the fluctuation induced barrierless process occurs faster than the process I mediated recombination, it should be discernible as a separate process. If process I which is governed by the distribution of barriers determined by the mean displacements of the CS, is much slower than the depletion of the gray zone fluctuation induced recombination then the latter process should have a time dependence that directly reflects the fluctuation spectrum of the gray zone CS. HbO_2 has several geminate recombination processes. There is one very prominent process that decays over a few hundred picoseconds and accounts for 40 to 60% of the re-

combination. Our preliminary results [15] indicate that this process remains relatively unchanged from ambient temperatures down to below 150 K. At 100 K it is no longer detectable. It appears that it stops rather abruptly in contrast to the progressive slowing expected for process I recombination. It is possible that this fast phase of recombination is an example of the fluctuation induced gray zone recombination. This process is not observed for Mb. A possible explanation based on the difference in the Raman spectra of Mb* and Hb*, is that the distribution of proximal parameters for Mb* contains fewer gray zone values.

The absence of the 100 ps geminate phase at room temperature in MbO_2 [13,15] and several lower vertebrate HbO_2s [13,49] has been explained [13,39,41,49] in terms of the respective photoproducts having a lower frequency $\nu(Fe-His)$ than for HbA. In addition those hemeproteins that display a reduced or absent 100 ps geminate phase also show a reduced or absent 100 ns geminate phase as in the case of Mb. The yield for both geminate processes appears to correlate with the proximal parameters as reflected in $\nu(Fe-His)$ [27]. A current view [3,13] of the origin of the 100 ps and 100 ns geminate processes is that the faster one corresponds to process I involving the encounter complex (contact pair) and the nanosecond one originates from much more separated ligand heme species (there is evidence to suggest that the ligand may be localized at the back of the heme pocket [50]). An interesting but by no means proven alternative interpretation of the ambient temperature geminate processes is that the sub 5 ps process is the barrierless process involving the red edge CS (no interconversion of CS on this time scale), the 100 ps process is the gray zone fluctuation mediated barrierless process (either no interconversion within either tier or interconversion of only the second tier CS) and the nanosecond process is the barrier controlled process I but with the distribution of barriers averaged by large scale fluctuations that interconvert the second and first tier proximal CS. It must be assumed that the fluctuation driven interconversion of the CS takes place on a time scale that is longer than the 100 ps process but less than 100 ns. The fluctuations driving the gray zone process are different in that they modulate the displacement of the iron within a given CS. The time course for the

gray zone process represents the depletion of the gray zone CS which would have to occur faster than the interconversion of the CS by the more global fluctuations. These slower global fluctuations might also be responsible for mediating the movement of the ligand away from the immediate vicinity of the iron. It should be noted therefore that this alternative assignment is not mutually exclusive with the idea that the slower process involves a more separated geminate pair than for the faster processes.

References

[1] E. Antonini and M. Brunori, Hemoglobin and Myoglobin in their Reactions with Ligands (North-Holland, Amsterdam, 1971).

[2] R.H. Austin, K.W. Beeson, L. Eisentein, H. Frauenfelder and I.C. Gunsalus, Biochemistry 14 (1975) 5355.

[3] K.A. Jongeward, D. Magde, D.J. Taube, J.C. Marsters, T.G. Traylor and V.S. Sharma, J. Am. Chem. Soc. 110 (1988) 380.

[4] L.P. Murray, J. Hofrichter, E.R. Henry, M. Ikeda-Saito, K. Kitageshi, T. Yonetani and W.A. Eaton, Proc. Natl. Acad. Sci. USA 85 (1988) 2151.

[5] B. Alpert, S.E. Mohsni, L. Lindqvist and F. Tfibel, J. Chem. Phys. 64 (1979) 11.

[6] D.A. Duddel, R.J. Morris and J.T. Richards, Chem. Soc. Chem. Commun. (1979) 75.

[7] J.M. Friedman and K.B. Lyons, Science 284 (1980) 570.

[8] E.R. Henry, J.H. Sommer, J. Hofrichter and W.A. Eaton, J. Mol. Biol. 166 (1983) 443.

[9] J.W. Petrich, C. Pyart and J.L. Martin, Biochemistry 27 (1988) 4049.

[10] J.W. Petrich and J.L. Martin, Chem. Phys. 131 (1989) 31.

[11] P.A. Cornelius, W.A. Steele, D.A. Chernoff and R.M. Hochstrasser, Proc. Natl. Acad. Sci. USA 78 (1981) 7526.

[12] P.A. Cornelius, R.M. Hochstrasser and W.A. Steele, J. Mol. Biol. 163 (1983) 119.

[13] J.M. Friedman, T.W. Scott, G.J. Fisanick, S.R. Simon, E.W. Findsen, M.R. Ondrias and V.W. Macdonald, Science 229 (1985) 187.

[14] H. Frauenfelder and P.G. Wolynes, Science 229 (1985) 337.

[15] M.R. Chance, S.H. Courtney, M.D. Chavez, M.R. Ondrias and J.M. Friedman, Biochemistry 29 (1990) 5537.

[16] M.R. Ondrias, T.W. Scott, J.M. Friedman and V.W. Macdonald, Chem. Phys. Letters 112 (1984) 351.

[17] P.J. Steinbach, A. Ansari, J. Berendzen, D. Bruanstein, K. Cu, B. Cowen, D. Ehrenstein, H. Frauenfelder, J.B. Johnson, D.C. Lamb, S. Luck, J.R. Mourant, G.U. Nienhaus, P. Ormos, R. Philipp, A. Xie and R. Young, Biochemistry 30 (1991) 3988.

[18] T.G. Traylor, D.J. Taube, K.A. Jongeward and D. Magde, J. Am. Chem. Soc. 112 (1990) 6875.

[19] T. Iizuka, H. Yamamoto, M. Kotani and T. Yonetani, Biochim. Biophys. Acta 371 (1974) 126.

[20] W.A. Eaton, L.K. Hanson, P.J. Stepens, J.C. Sutherland and J.B. Dunn, J. Am. Chem. Soc. 100 (1978) 4991.

[21] B.F. Campbell, M.R. Chance and J.M. Friedman, Science 238 (1987) 373.

[22] N. Agmon, Biochemistry 27 (1988) 3507.

[23] M.D. Chavez. S.H. Courney, M.R. Chance, D. Kiula, J. Nocek, B.M. Hoffman, J.M. Friedman and M.R. Ondrias, Biochemistry 29 (1990) 4844.

[24] D.L. Rousseau and J.M. Friedman, in: Biological Applications of Raman Spectroscopy, vol. 3, ed. T.G. Spiro (Wiley, New York, 1988) pp. 133–215.

[25] J.M. Friedman, D.L. Rousseau, M.R. Ondrias and R.A. Stepnoski, Science 218 (1982) 1244.

[26] J.M. Friedman, Science 228 (1985) 1273.

[27] J.M. Friedman, B.F. Campbell and R. Noble, Biophys. Chem. 37 (1990) 43.

[28] O. Bangcharoenpaurpong, K.T. Schomacker and P.M. Champion, J. Am. Chem. Soc. 106 (1984) 5688.

[29] M. Sassaroli, S. Dasgupta and D.L. Rousseau, J. Biol. Chem. 261 (1986) 376.

[30] L. Powers, B. Chance, M. Chance, B. Campbell, J. Friedman, A. Naqui, K.S. Reddy and Y. Zhow, Biochemistry 26 (1987) 4785.

[31] J.M. Friedman and M.R. Ondrias, Proc. SPIE 1055 (1989) 216.

[32] D. Rousseau and P.V. Argade, Proc. Natl. Acad. Sci. USA 83 (1986) 1310.

[33] A. Ansari, PhD Thesis, University of Illinois at Urbana-Champaign (1988).

[34] H. Frauenfelder, N.A. Alberding, A. Ansari, D. Braunstein, B.R. Cowen, M.K. Hong, I.E.T. Iben, J.B. Johnson, S. Luck, M.C. Marden, J.R. Mourant, P.I. Ormos, L. Reinisch, R. Scholl, A. Schulte, E. Shyamsunder, L.B. Sorensen, P.J. Steinbach, A.H. Xie, R.D. Young and K.T. Yue, J. Phys. Chem. (1990) 1024.

[35] A. Ansari, J. Berendzen, S.F. Bowne, H. Frauenfelder, I.E.T. Iben, T.B. Sauke, E. Shyamsunder and R.D. Young, Proc. Natl. Acad. Sci. USA 82 (1985) 5000.

[36] A. Ansari, E.E. Di Iorio, D. Dlott, H. Frauenfelder, I.E.T. Iben, P. Langer, H. Roder, T.B. Sauke and E. Shyamsunder, Biochemistry 25 (1986) 3139.

[37] N. Agmon and J.J. Hopfield, J. Chem. Phys. 79 (1983) 2042.

[38] T.W. Scott and J.M. Friedman, J. Am. Chem. Soc. 106 (1984) 5677.

[39] E.W. Findsen, J.M. Friedman, M.R. Ondrias and S.R. Simon, Science 229 (1985) 661.

[40] E.W. Findsen, T.W. Scott, M.R. Chance, J.M. Friedman and M.R. Ondrias, J. Am. Chem. Soc. 107 (1985) 3355.

[41] M. Sassaroli and D. Rousseau, Biochemistry 26 (1987) 3092.

[42] P.M. Champion and V. Srajer, Bull. Am. Phys. Soc. A 36 (1991) 761.

[43] E.W. Findsen, J.M. Friedman and M.R. Ondrias, Biochemistry 87 (1987) 8719.

[44] B.D. Olafson and W.A. Goddard III, Proc. Natl. Acad. Sci. USA 74 (1977) 1315; W.A. Goddard III and B.D. Olafson, Biochemical and Clinical Aspects of Oxygen, ed. W.S. Caughey (Academic Press, New York, 1979) p. 87.

[45] M. Karplus, in: Hemoglobin and Oxygen Binding, ed. C. Ho (Elsevier, Amsterdam, 1982) p. 3.

[46] A. Szabo, Proc. Natl. Acad. Sci. USA 75 (1978) 2108.

[47] I.E.T. Iben, B.R. Cowen, R. Sanchez and J.M. Friedman, Biophys. J. 59 (1991) 908.

[48] B.R. Cowen, PhD Thesis, University of Illinois, Urbana (1990).

[49] J.M. Friedman, S.R. Simon and T.W. Scott, Copeia 3 (1985) 679.

[50] K.A. Johson, J.S. Olson and G.N. Phillips, J. Mol. Biol. 192 (1986) 133.